SAE TECHNICAL PAPER SERIES

2007-01-3647

Automated Steering Controller for Vehicle Testing

David R. Mikesell, Anmol S. Sidhu and Dennis A. Guenther
The Ohio State University

Gary J. Heydinger and Ronald A. Bixel
SEA Ltd

14th Asia Pacific Automotive Engineering Conference
Hollywood, California, USA
August 5-8, 2007

SAE International™

400 Commonwealth Drive, Warrendale, PA 15096-0001 U.S.A. Tel: (724) 776-4841 Fax: (724) 776-0790 Web: www.sae.org

ISSN 0148-7191

Printed in USA

2007-01-3647

Automated Steering Controller for Vehicle Testing

David R. Mikesell, Anmol S. Sidhu, Dennis A. Guenther
The Ohio State University

Gary J. Heydinger, Ronald A. Bixel
SEA Ltd.

ABSTRACT

Automating road vehicle control can increase the range and reliability of dynamic testing. Some tests, for instance, specify precise steering inputs which human test drivers are only able to approximate, adding uncertainty to the test results. An automated steering system has been developed which is capable of removing these limitations. This system enables any production car or light truck to follow a user-defined path, using global position feedback, or to perform specific steering sequences with excellent repeatability. The system adapts itself to a given vehicle s handling characteristics, and it can be installed and uninstalled quickly without damage or permanent modification to the vehicle.

INTRODUCTION

Each year millions of dollars and countless man-hours are spent around the world by automotive manufacturers, government agencies, consumer groups, and others doing road vehicle testing. To date, most of this test driving is left in the hands of human drivers. Though human drivers can readily handle very complex tasks and provide holistic feedback as to vehicle response, such capabilities are not always needed. Much testing consists of simple, repetitive maneuvers which are not only tedious but can also be hard on the body. Some tests are dangerous enough to warrant a helmet, five-point harness, and vehicle outriggers. Others are precluded altogether due to potential harm to the occupants.

The steering controller is part of an Automated Test Driver (ATD), incorporating steering, brake, and throttle control to autonomously conduct open- and closed-loop dynamic maneuvers. Though automated vehicle control is not in itself new, the proposed system aims for distinction in its portability, ease and transparency of installation, and its ability to adapt to the handling characteristics of each vehicle.

Similar devices can be found in technical or commercial literature. Two European firms market a handwheel controller, one with some possibility for coordination with a brake actuator, but no claims are made for driverless testing [1,2]. Volkswagen developed a very capable autonomous system, but it is too cumbersome to fit in small cars [3,4]. Others are vehicle-specific designs which modify or bypass stock throttle, brake, or steering linkages, generally designing the control system around the performance of one particular vehicle (e.g., [5,6]).

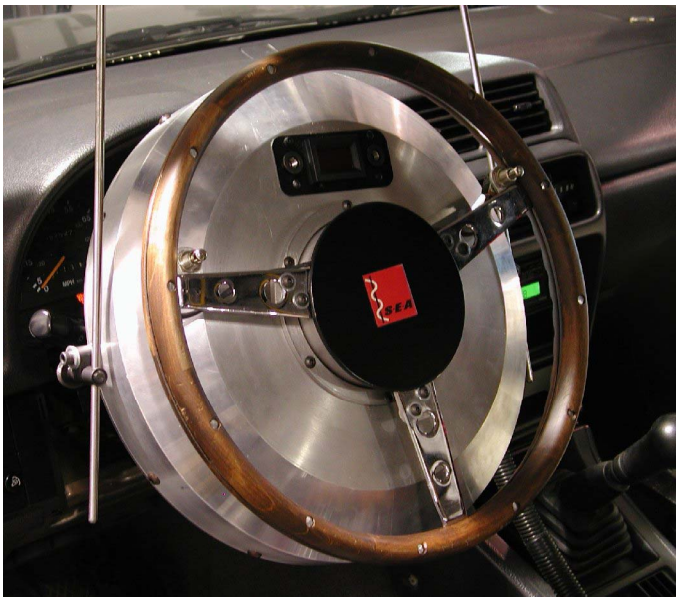

Fig. 1: SEA Ltd., handwheel unit

GOALS

The automated steering controller is based on a handwheel actuator designed and manufactured by SEA Ltd., (Fig. 1) [7,8,9]. Originally developed to precisely execute open-loop handwheel commands, the capability was then expanded to include path following. In [10], Sidhu et. al. develop and implement a preview-type algorithm incorporating the SEA actuator which performed well in road tests at low speeds.

This paper describes the extension of the above work in the following directions. First, the sensor suite and processing hardware has been condensed to a smaller and easier-to-install package. Second, the control algorithm is optimized to enable operation at higher speeds and appropriate gain scheduling rules were added.

HARDWARE

Global position feedback, originally fused from a combination of three separately-housed sensors, is now provided by the RT3002, a GPS/INS package from Oxford Technical Solutions (Fig. 2) [11]. This compact instrument, capable of 2 cm position and 0.1 deg heading accuracies, simplifies the sensor wiring and installation.

Fig. 2: RT3002 by OXTS

The supervisory and servo control functions, formerly split between two computers, have been consolidated into one National Instruments CompactRIO [12]. CompactRIO combines a 400 MHz processor running a real-time operating system with a 3M-gate FPGA (field-programmable gate array) to handle I/O processing and integer-based mathematical functions. Its small, lightweight, and robust packaging are well-suited for in-vehicle use.

An overview of the steering system hardware is shown in Fig. 3. Note that the car battery shown represents the 12V battery / alternator already in the vehicle, not a separate battery for this system.

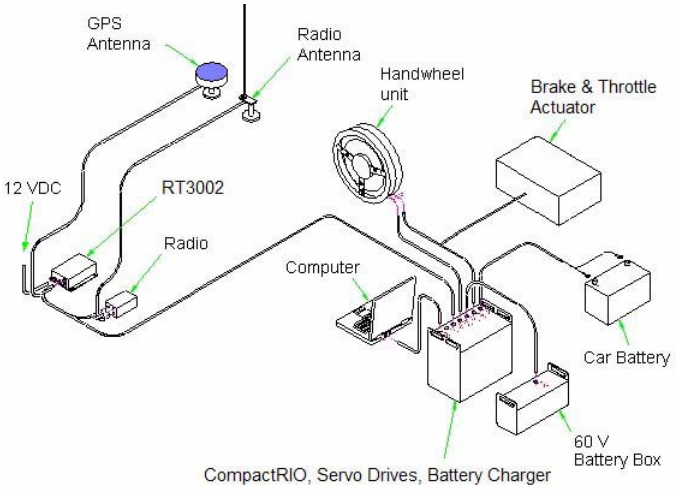

Fig. 3: System overview

STEERING CONTROL

PATH-FOLLOWING ALGORITHM

The algorithm developed by Sidhu is based on heading error control. A goal point on the intended path is first selected, the point which is a given distance (lookahead) from the current vehicle position (Fig. 4). Here we assume that the path is defined as a series of discrete points, rather than a continuous function. This allows the user to easily define an arbitrary path.

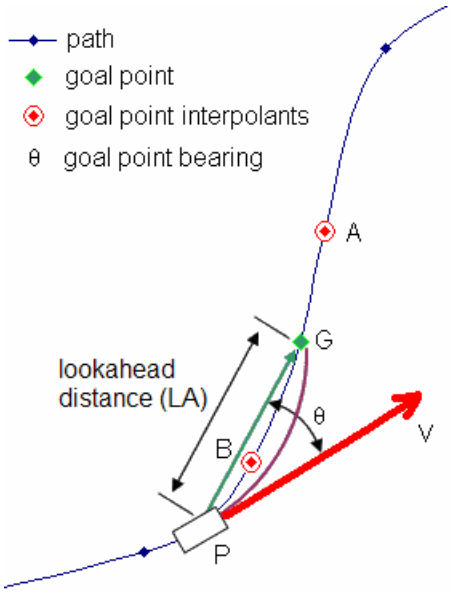

Fig. 4: Goal point calculation

In Fig. 4, points A and B are defined path points. G is the goal point, the point interpolated between A and B which is exactly one lookahead distance from the vehicle. The controller then determines the angle between the vehicle heading and the goal point bearing (θ in Fig. 4), termed the `headingerror` PD control is applied to this heading error, and the result becomes the steering command. See Eqn. (1), where δ_{hw} is handwheel steering angle.

$$\delta_{hw} = K_p \theta + K_d \frac{d\theta}{dt} \qquad (1)$$

In other words, the PD operator acts to drive the difference between vehicle heading and the bearing of the goal point to zero. Though the basic calculation is simple, other subtleties must be included to adapt the controller for different speeds, path curvatures, and different vehicles.

A number of preview-based algorithms for path-following have been explored over the past twenty years, including follow-the-carrot [13], pure pursuit [14], and vector pursuit [15]. The pure pursuit method, for instance, geometrically computes the Ackerman steering angle required to traverse the arc between P and G. Pure

pursuit is limited in two ways: first, its only tuning parameter is lookahead distance; second, its path-following accuracy is tied to the Ackerman angle, which is typically accurate only at low speeds. Sidhu's method captures the simplicity of pure pursuit while giving additional tuning options to optimize performance on a given vehicle and account for moderate slip situations at higher speeds.

The preview-based nature of Sidhu's algorithm makes it inherently feed-forward. The algorithm does not act on current lateral deviation from the path, but rather on anticipated future deviation. Further improvement may be possible by analyzing the path curvature at or beyond the goal point and modifying the control law accordingly, but this method has not yet been explored.

PARAMETER ADAPTATION

In order to investigate speed-dependent or vehicle-dependent parameter adaptation, the system was modeled in LabVIEW to conduct path-following simulations. Simulations were performed on four different vehicles in an attempt to classify behavior by vehicle type or characteristic. The vehicles used are listed in Table 1.

Table 1: Vehicles used in simulation

	Mass (kg)	Wheel-base (m)	CG Height (mm)
1987 Hyundai Excel	1299	2.380	539
1994 Ford Taurus	1667	2.690	542
1997 Jeep Cherokee	1663	2.578	682
2003 Ford Expedition	2591	3.019	709

Vehicle lateral dynamics were modeled with a 3-DOF state-space system including roll motion and compensation for multiple steering and suspension compliances (see Appendix). Because tire cornering force was modeled as a linear function of slip angle, simulations were constrained to maneuvers designed for lateral acceleration at or below 0.3 g. Steering actuator and linkage dynamics were modeled using a 2nd-order transfer function developed by Brown [5].

Paths for Simulation

The paths used for these simulations were similar to those shown in Fig. 5. The paths start at (0,0) and go northward. All paths were traveled at a constant speed, and all involved a rightward side shift of 10 m.

In order to fairly compare these vehicles across a wide range of speeds, the same path could not be used for all trials. Thus the transition between the two "lanes" was based on a circular arc, the radius of which was designed to achieve a given nominal centripetal acceleration.

Three different centripetal acceleration values were used for paths: 0.5, 1.0, and 2.0 m/s^2. Vehicles closely tracking the path would experience a maximum lateral acceleration close to the path design value; poorly tracking vehicles could experience substantially higher lateral accelerations. Therefore the trials run with optimal results stayed well within the linear, valid region of the vehicle model. (Though lateral acceleration is a combination of true lateral and centripetal movements, the centripetal effect is dominant.)

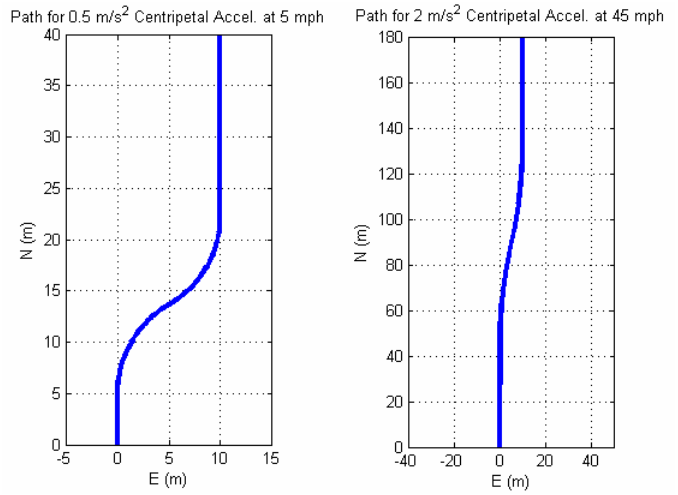

Fig. 5: Sample paths

Parameter Variation

Three parameters are available to determine the behavior of the proposed steering algorithm: lookahead (*LA* in Fig. 4), and K_p and K_d from Eqn. (1). Based on prior experience [10], the dominant parameters are lookahead and proportional gain (K_p), with derivative gain (K_d) contributing a secondary effect. Therefore, though all trials were run using multiple values of K_d, the trials focused on variation of the first two parameters.

The optimal combination of proportional gain (K_p) and lookahead (LA) was computed for each trial based on two criteria. The first criterion was *path-following error*, which was calculated by finding the total area between the intended path and the actual vehicle trajectory, then dividing by the length of the path traveled.

The second criterion was *controller stability*. An FFT was calculated for the steering command on each trial. From observation, there was a critical frequency which corresponded to excessive steering oscillation on these maneuvers. Trials revealing a spectral magnitude higher than a given threshold at the critical frequency were discarded, even if they followed the path more closely than the others.

The controller stability criterion was only used on trials above 15 mph (24 kph). Below this speed, the critical

frequency was too close to the frequencies otherwise required for completing the steering maneuver.

SIMULATION RESULTS

Trials were conducted at multiples of 5 mph (8 kph) for combinations of integer values of K_p and LA. Sample results for one such test, for the Jeep Cherokee tested at 15 mph on a path requiring 0.5 m/s^2 centripetal acceleration, are shown in Fig. 6. The arrow points to the asterisk indicating the trial with lowest error, denoting the optimal combination of K_p and LA for this path and speed.

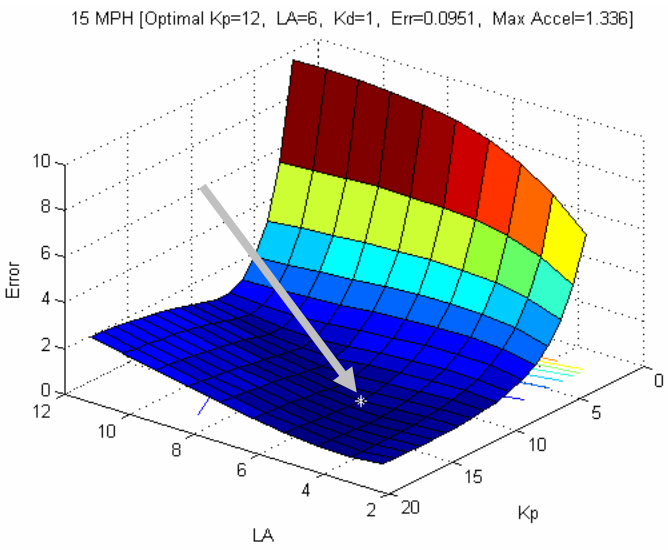

Fig. 6: Sample simulation result

Evaluation of Derivative Gain (K_d)

Fig. 7 and Fig. 8 show the effect of K_d on optimal path tracking error for two different vehicles. (The error value plotted at each speed represents the lowest error for any tested combination of control parameters.) Some derivative gain is clearly helpful, especially at higher speeds. Larger K_d yields slightly better results above 55 mph, but this margin is negligible.

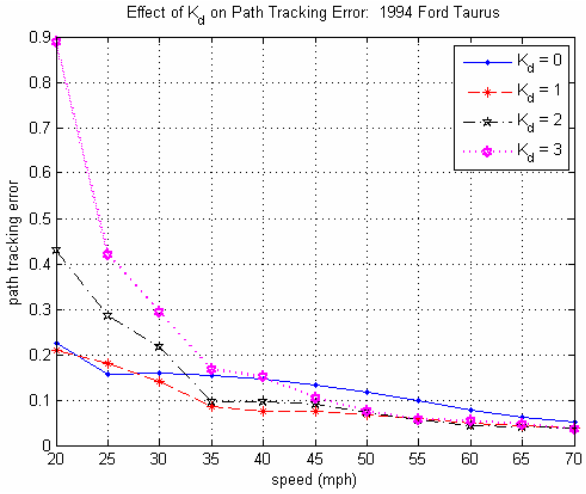

Fig. 7: Effect of K_d on path tracking error

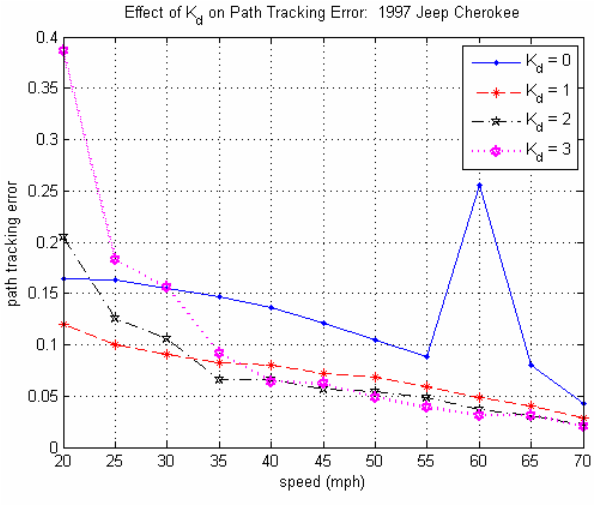

Fig. 8: Effect of K_d on path tracking error

For both the Taurus and Cherokee, a derivative gain of 1 gives very good results across the entire range of speeds, including results for lower speeds not shown here. Therefore K_d = 1 will be used for all subsequent analysis, and further control adaptation will focus on the effects of proportional gain (K_p) and lookahead (LA).

Evaluation of Lookahead (LA)

As can be seen from the Taurus results in Fig. 9, optimal lookahead is well-represented by a linear fit when plotted versus speed. This was also the case for the other vehicles simulated.

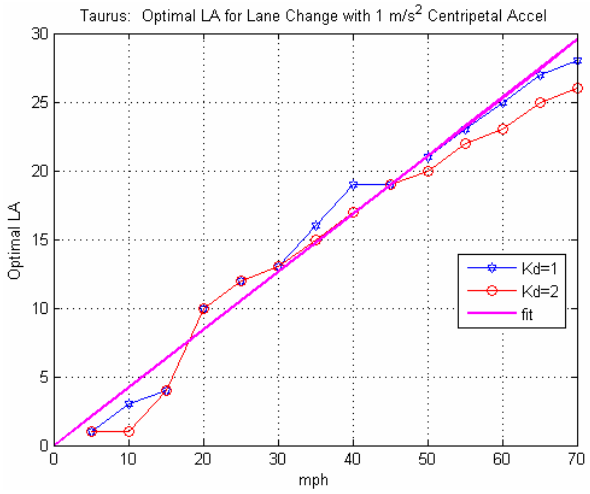

Fig. 9: Optimal lookahead for Taurus

When the linear fits for the four tested vehicles are overlaid (Fig. 10), it becomes clear that optimal lookahead is only weakly dependent on vehicle type, if at all. One curve fit (Eqn. (2)) would suffice for the Taurus, Jeep, and Excel. The Expedition, 55% heavier than the next closest test vehicle, may benefit from slightly longer lookahead due to its mass-related slower response (Eqn. (3)).

$$LA(m) = 0.40mph + 0.2 \quad (2)$$

$$LA(m) = 0.44mph + 0.2 \quad (3)$$

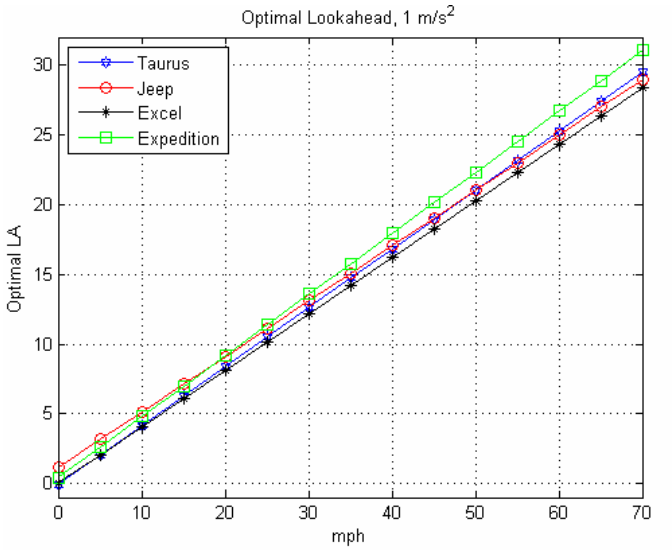

Fig. 10: Optimal lookahead vs. speed, 1 m/s^2

The results shown in Fig. 10 were for simulations run on a path designed for 1 m/s^2 centripetal acceleration. When compared to results for 0.5 and 2 m/s^2, the curve fits are slightly different (Fig. 11). No results are shown for 2 m/s^2 below 10 mph, because lateral acceleration this high is not realistic at lower speeds.

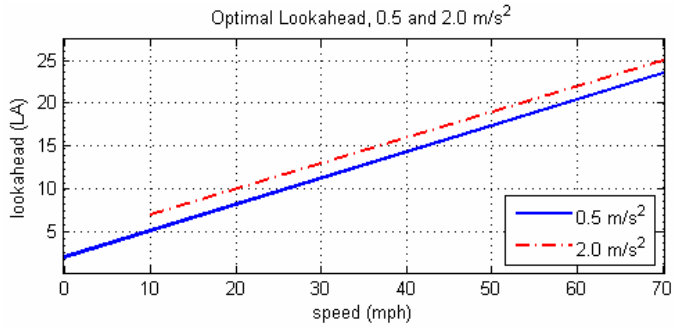

Fig. 11: Optimal lookahead, 0.5 and 2 m/s^2

Again the trends are roughly the same for each vehicle. Because the difference between these fits is relatively small, the 1 m/s^2 settings would likely give acceptable results for a wide variety of paths. For cases where very close path tracking is required, however, the path could be preprocessed to determine how aggressive the lateral acceleration is at each section, and the lookahead rule could be adjusted accordingly.

Evaluation of K_p

Simulation results for optimal proportional gain (K_p) are difficult to interpret (Fig. 12, 5-70 mph). The relationship of K_p to speed is not linear, and this parameter varies quite a bit with vehicle type.

Significantly higher gains were found to yield the lowest path-following error at low speeds. But this trend should not be extended all the way to zero speed, because the vehicle must have some forward motion before the steering angle will have any effect on heading. Because of this, and to avoid excessive demands on the actuator, proportional gain at 0-5 mph should be linearly scaled up from zero to its otherwise optimal value.

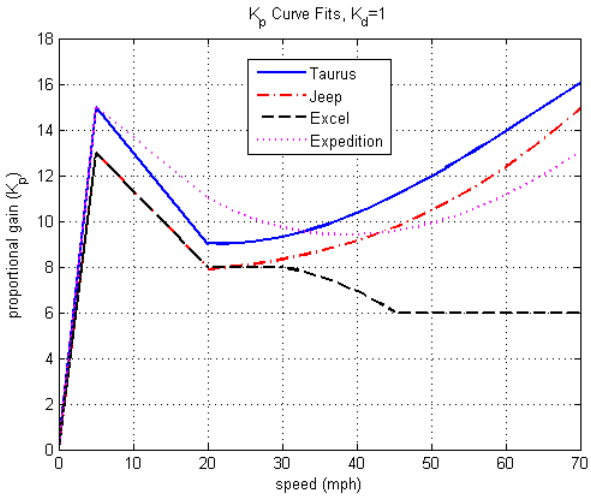

Fig. 12: Optimal proportional gain (K_p) by simulation, 0-70 mph

While K_p trends for the Taurus, Jeep, and Expedition are similar, the Excel's curve deviates sharply at speeds above 30 mph. Plotting the error surface for the Excel at one sample higher speed, shown in Fig. 13, reveals that slightly higher path-following error is indeed present for K_p greater than 6.

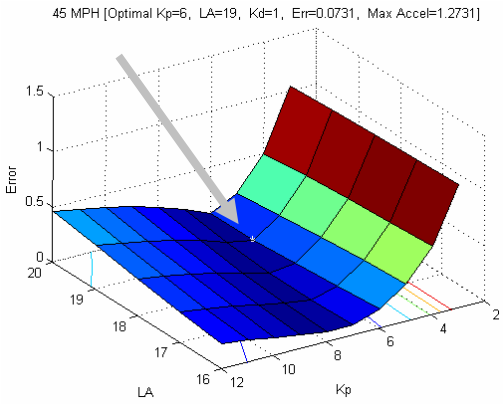

Fig. 13: Excel error surface at 45 mph

Judging by the two simulation results shown in Fig. 14 and Fig. 15, the Excel's problem with high gain at higher speeds can be traced to steering instability. Fig. 14 shows path following performance and handwheel angle for the 45 mph test using optimal control parameters; Fig. 15 shows results when (only) the K_p is increased to 10, a value which is near-optimal for the other simulated vehicles. Fig. 15 shows that the Excel still adheres well to the path using the higher K_p , but the plot of

handwheel angle reveals a marked oscillation not present in the optimal case (Fig. 14).

Higher gains excite some system mode in the Excel simulation which is significantly different than in the other vehicles. The low mass of the Excel is certainly a factor, being 364 kg (22%) lighter than the next closest vehicle.

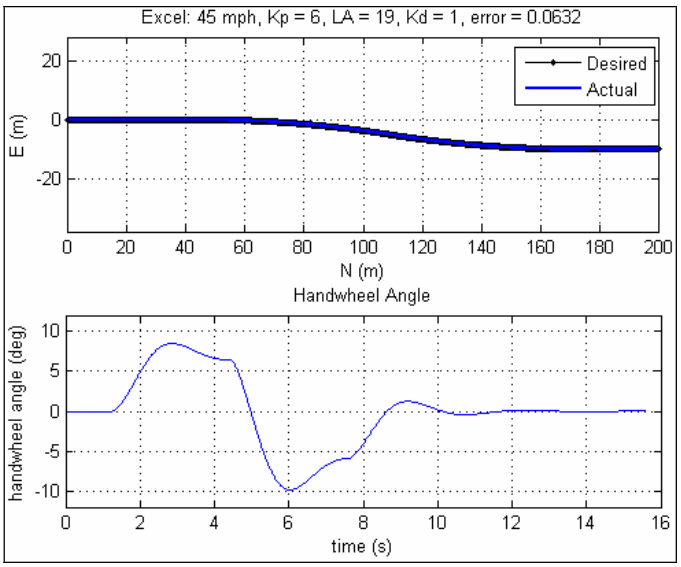

Fig. 14: Excel test manv. at 45 mph, Kp = 6 (optimal)

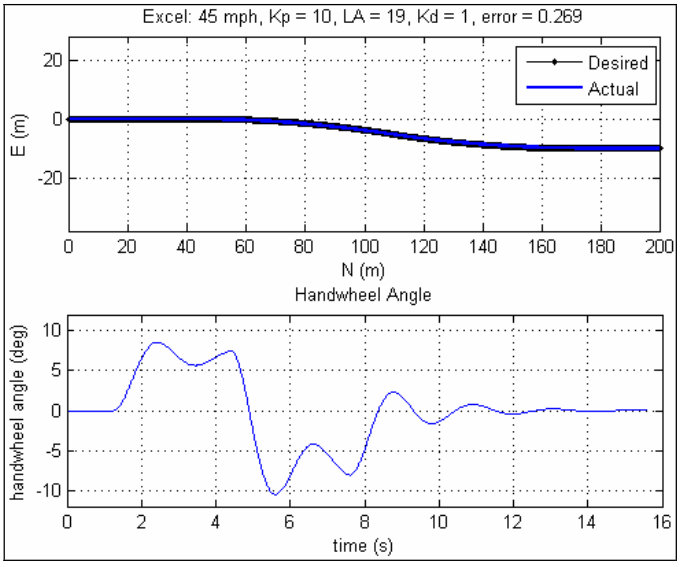

Fig. 15: Excel test manv. at 45 mph, Kp = 12

In contrast to the empirical simulation-based approach to gain selection, a more academic approach to selecting proportional gain begins with yaw gain. Yaw gain is defined by Gillespie [16] as the ratio of yaw rate to steering angle, r/δ_K. The essence of the control problem lies in understanding this ratio for a given vehicle. The algorithm has chosen our goal point based on the optimal lookahead distance. Then based on vehicle speed, one particular yaw rate will cause the vehicle to intercept this goal point.

Finally, the controller must order the proper steering angle to achieve this desired yaw rate. This is where, for the proposed control law, proportional gain becomes involved. Begin with Eqn. (1), neglecting for now the derivative term (variable definitions are in the Appendix):

$$\delta_{hw} = K_p \theta \tag{4}$$

The desired yaw rate (r_{des}) is implicit in bearing error θ. $r_{des} = \theta / t$, where t is the time until the vehicle reaches the goal point. This t can be calculated as the ratio of the lookahead distance to vehicle speed. Rearranging this, one can calculate a theoretical *Kp* value as shown in Eqns. (5,6). Note that yaw gain, the denominator term in parentheses in Eqn. (6), is stated in terms of handwheel angle rather than tire angle.

$$\theta = r_{des} t = r_{des} \frac{LA}{vel} \tag{5}$$

$$K_p = \frac{\delta_{hw}}{\theta} = \left(\frac{\delta_{hw}}{r_{des}} \right) \frac{vel}{LA} = \left(\frac{1}{r_{des} / \delta_{hw}} \right) \frac{vel}{LA} \tag{6}$$

Yaw gain is dependent on many factors, including vehicle speed, mass, wheelbase, and tire properties. These properties are typically not available for every test vehicle, making theoretical determination difficult. But any one of the three common steady-state test maneuvers can be used to quickly identify the yaw gain for a vehicle [17]:

- Slowly increasing steer with constant speed
- Slowly increasing speed with constant steer
- Constant radius test with slowly increasing speed and steer

A sample calculation can be made using data from an experimental test shown in Fig. 17 (2 m/s^2 lateral shift at 20 mph, LA = 5 m). The measured yaw rate, goal point bearing, and handwheel angle for this test are shown in Fig. 16. Though not a steady state test, the ~1.5-second period around time = 15 sec approaches this.

First estimate the yaw gain from Fig. 16 at time = 15 sec.

$$\frac{r}{\delta_{hw}} = \frac{13\,\text{deg}/s}{83\,\text{deg}} = 0.157 s^{-1} \tag{7}$$

This yaw gain was similarly calculated from experimental results on the same vehicle and same speed at 1 m/s^2 and 3 m/s^2. Results (0.153 and 0.155s^{-1}, respectively) were within 3% of the value shown in Eqn. (7).

Now calculate a theoretical Kp using Eqn. (6) with the known lookahead and velocity:

$$K_p = \left(\frac{1}{0.157 s^{-1}}\right)\frac{8.9 m/s}{5m} = 11.4 \qquad (8)$$

This compares favorably with the optimal K_p of 12 calculated in simulation for this scenario (Fig. 20). Yet since yaw gain is a steady-state characteristic and path-following employs generally transient steering, the relationship shown in Eqn. (6) can be only a guideline in system tuning.

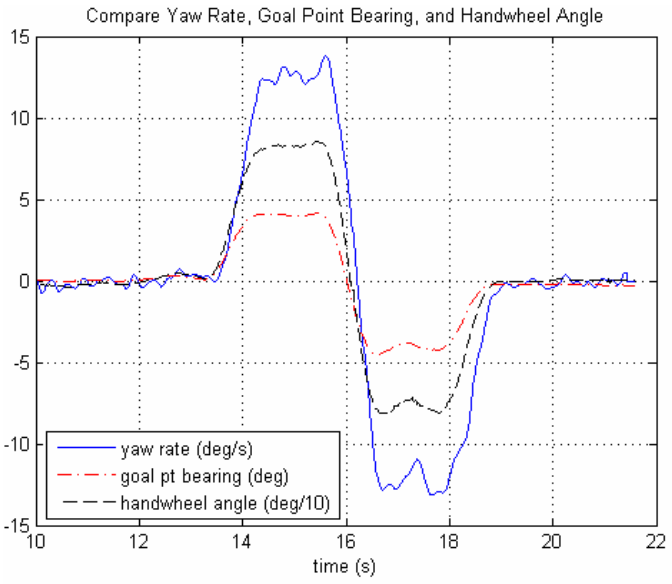

Fig. 16: Yaw rate, goal pt. brg., handwheel angle

VALIDATION

The two vehicles listed in Table 2 were tested on a 220m x 160m asphalt surface. Due to the surface's small size, validation was restricted to tests 30 mph (48 kph) and below. Sufficient vehicle data was available for comparative simulations of the Honda CR-V [18], but not for the Ford F-150. It should be noted that the CR-V test vehicle tires did not match the reference tires, and not all simulation parameters were available, so tire stiffness data and some compliance parameters were estimated.

Lateral shift maneuvers identical to those simulated were performed on the test vehicles. Tests were conducted at 10, 20, and 30 mph to determine the optimal lookahead and proportional gain for side shifts at 1, 2, and 3 m/s^2. Speed control was performed by the ATD brake and throttle actuator. All tests were conducted with K_d = 1.

Sample results are shown in Fig. 17 and Fig. 18 for a test at 20 mph with a curve designed for 2 m/s^2 lateral acceleration. This test shown uses the gains experimentally found to be optimal for this speed and path, K_p = 18 and LA = 5 m. At this scale, traces for the desired path and actual performance are indistinguishable. Once the vehicle enters the first curve, GPS reports that the maximum deviation from path is 25mm, roughly half of that sensor's nominal accuracy. Similar experimental results were obtained for all test points.

Table 2: Test Vehicles

	Mass (kg)	Wheel-base (m)	CG Height (mm)
1997 Honda CR-V	1529	2.621	633
1992 Ford F-150	2037	3.517	701

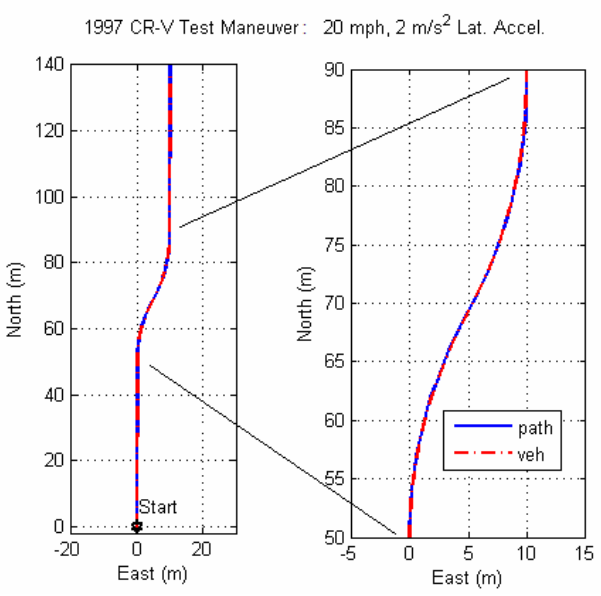

Fig. 17: CR-V sample test maneuver

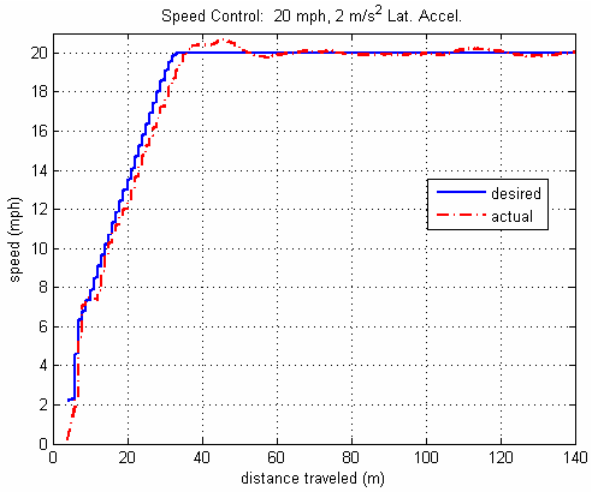

Fig. 18: CR-V sample test maneuver, speed control

Simulation and experimental results for optimal lookahead and proportional gain are shown in Fig. 19 and Fig. 20 below. Experimental tests were judged by the same criteria as previously explained for the simulation. Though the experimental tests were restricted to lower speeds, some comparisons may be made, and some trends are nonetheless clear.

Actual values for optimal lookahead (Fig. 19) are somewhat smaller than simulation values. The linear trend is still present, with roughly the same slope for all

values of centripetal acceleration. Experimental results for 2 and 3 m/s^2 show the same optimal LA, suggesting that these values may represent a lower bound.

The difference between simulation and experimental values may be attributable to excessive delay built into the simulation model. If the estimate of computation time, actuator dynamics, and tire lag exceeds the actual effective delay, then the simulator would require larger lookahead distances than are really necessary.

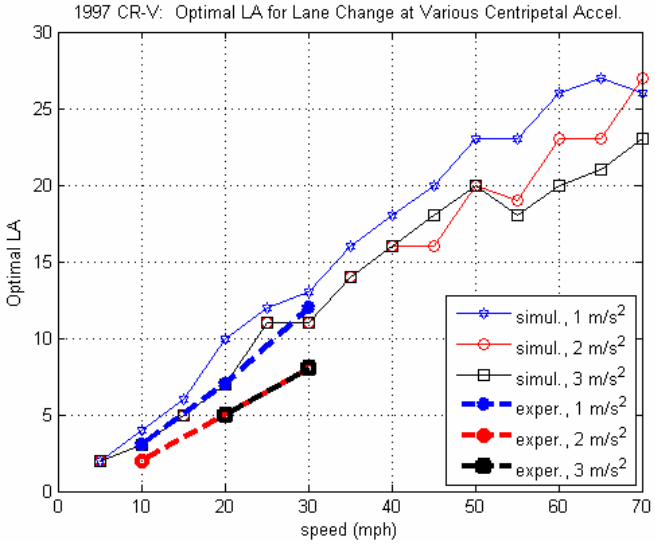

Fig. 19: Optimal LA for CR-V

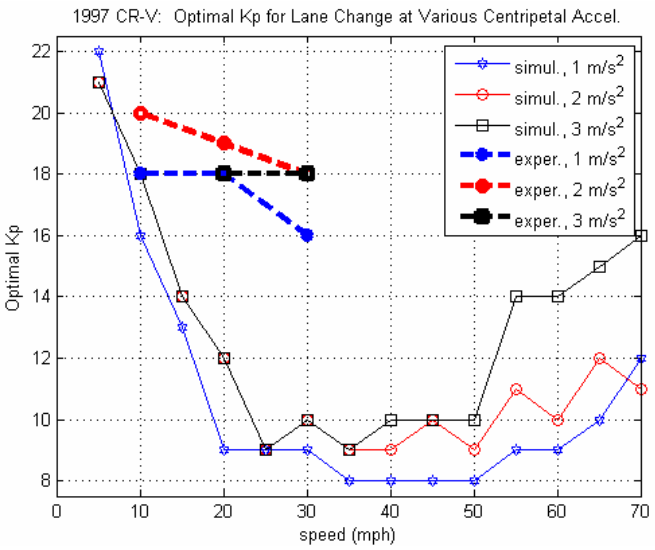

Fig. 20: Optimal Kp for CR-V

As for proportional gain, the values derived in simulation do achieve stable, reasonable results in practice, but not nearly as accurate as those found optimal by experiment. The downward trend with increasing speed is still present, though not as pronounced.

The discrepancy between the simulation and test results in Fig. 20 can be a result of multiple factors. First, the damping characteristic of the real mechanical system may not be adequately modeled. This allows the real vehicle to remain stable with high K_p values, gains which would cause unacceptable oscillation in the simulator. Second, related to the explanation given for the lookahead gains, excessive delay in the model would also tend to cause instability at lower gains than in the real vehicle. Based on these results, the mathematical model representing the control system and actuators could be reevaluated in an effort to improve the simulation.

Third, the values chosen as "optimal" from automatic computation of simulator results may not be so different from values with higher K_p. Examining the error surface on Fig. 6, for instance, one can see a broad plane of near-optimality for this simulation which extends to lower LA and higher K_p.

EXPERIMENTAL RESULTS: CR-V VS. F-150

Though simulation data is not available for the 1992 F-150 pickup truck, it is still instructive to compare the test data with results from the 1997 CR-V (Fig. 21). Optimal lookahead values are very close for the two vehicles. The longer wheelbase and higher yaw inertia of the F-150 may account for the slightly higher lookahead values shown for three data points.

Concerning proportional gain, values for the F-150 are in the same neighborhood as those for the CR-V. Both vehicles also show some tendency to prefer higher gains for more aggressive maneuvers. Note, too, that the optimal *Kp* at 20 mph is roughly 50% higher than the theoretical value of 11.4 previously calculated from yaw gain. This is perhaps attributable to the disparity between the "steady-state" origins of yaw gain and the transient nature of true path-following dynamics.

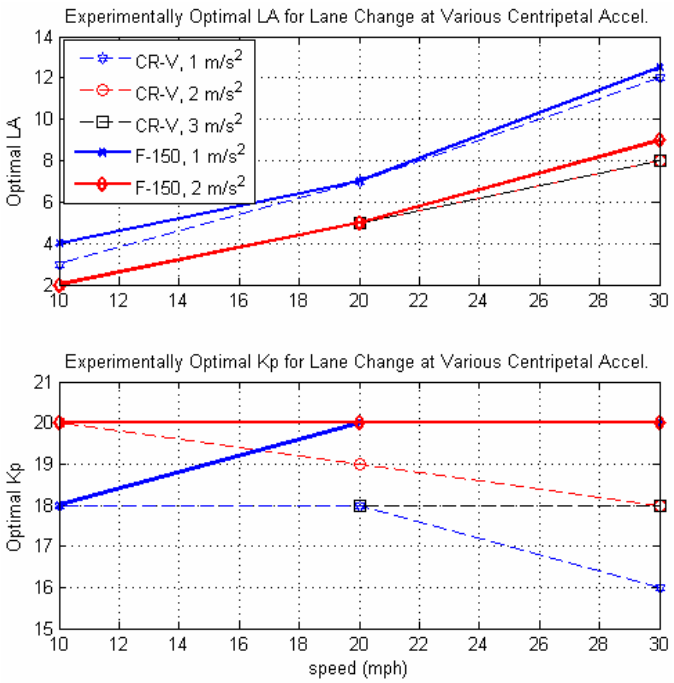

Fig. 21: CR-V vs. F-150, optimal parameters

After the lane-change-type tests were complete, the optimal parameters were employed on some random paths to verify performance and controller stability. Figures 22-24 show results from a sharp-featured path meant to test accuracy at low speed. The straight legs were traversed at 20 mph, slowing to 10 mph in between for the turns.

Gains were fixed at K_p = 20 and LA = 3, found optimal for the CR-V at 10 mph with 2 m/s^2 curves. Maximum deviation from path (as reported by GPS/INS) was 12 cm in the portion detailed in Fig. 23.

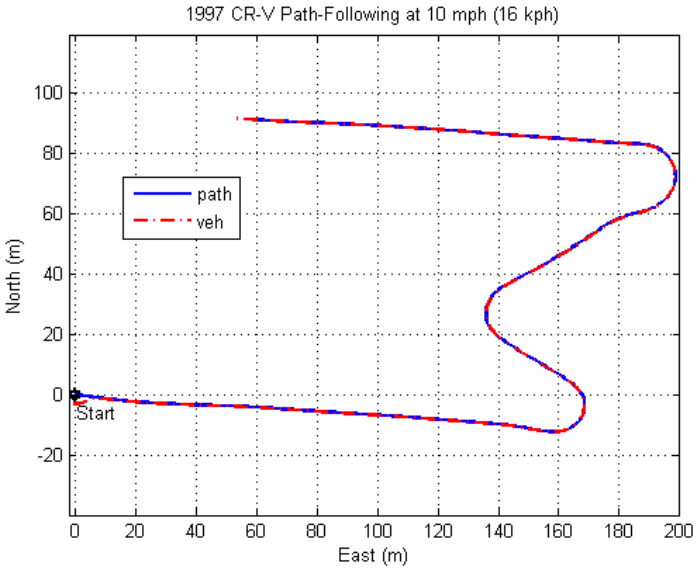

Fig. 22: CR-V path following at 10 mph (16 kph)

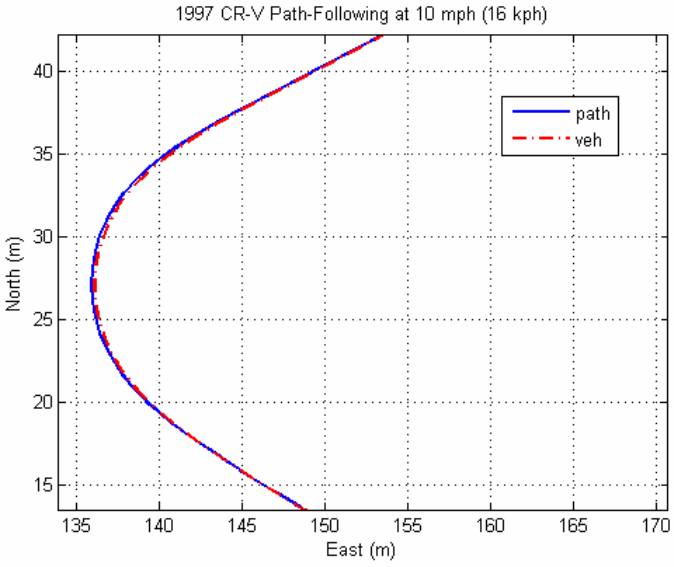

Fig. 23: CR-V path following at 10 mph, detail

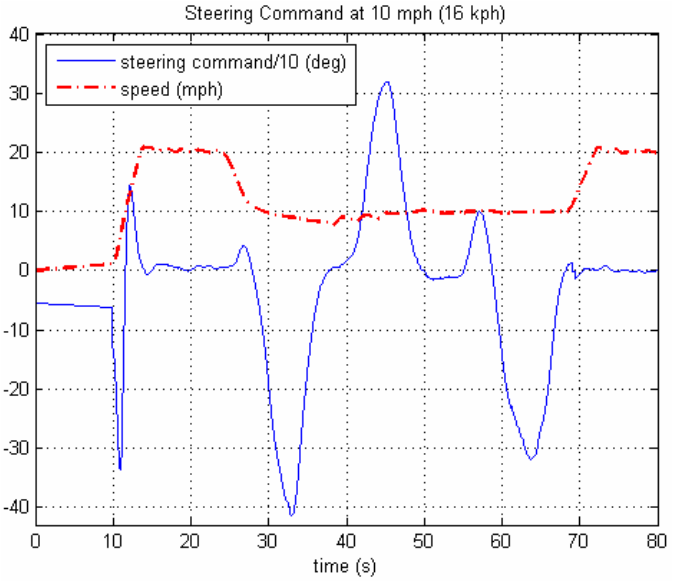

Fig. 24: CR-V path following at 10 mph (16 kph)

Results from a higher speed maneuver, which briefly reaches 0.5g lateral acceleration, are illustrated in Figs. 25-28. Maximum deviation for this path was 80 cm in the area shown in Fig. 26. Using the gains found optimal for 30 mph and 3 m/s^2 lateral acceleration (K_p = 18 and LA = 8 m), average deviation was around 36 cm for this test. While initial results for this aggressive path were promising, they would likely be improved with a proportional gain found optimal for the actual conditions.

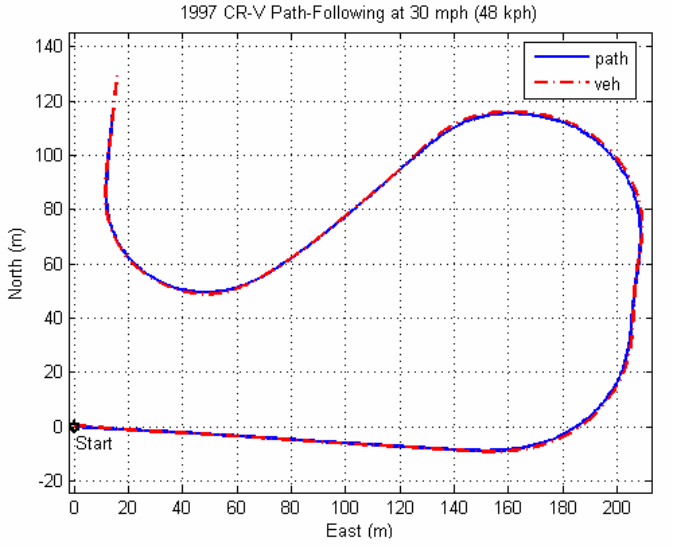

Fig. 25: CR-V path following at 30 mph (48 kph)

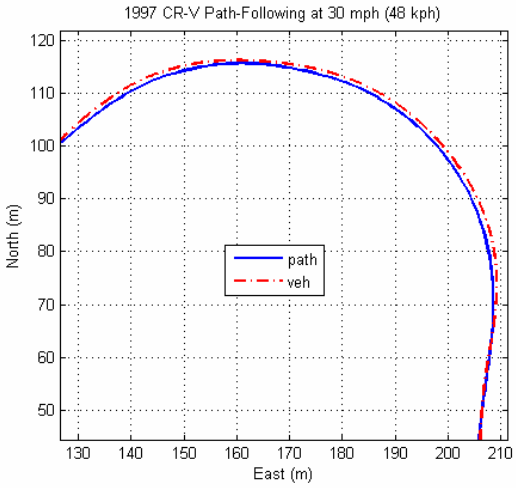

Fig. 26: CR-V path following at 30 mph, detail

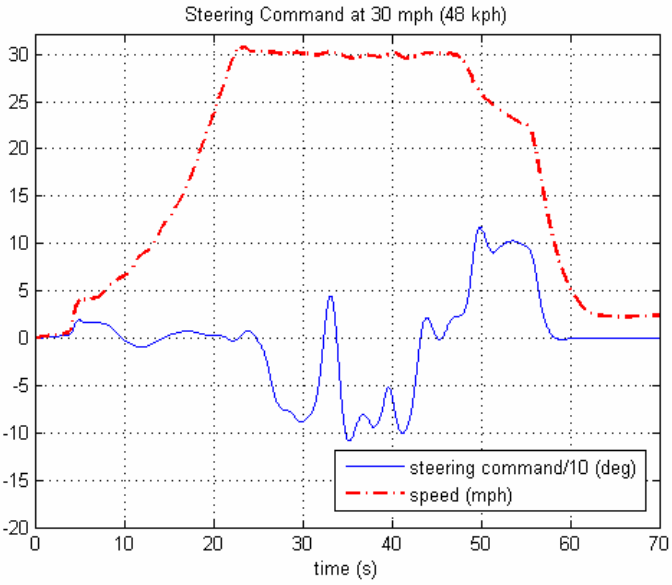

Figure 27: CR-V path following at 30 mph (48 kph)

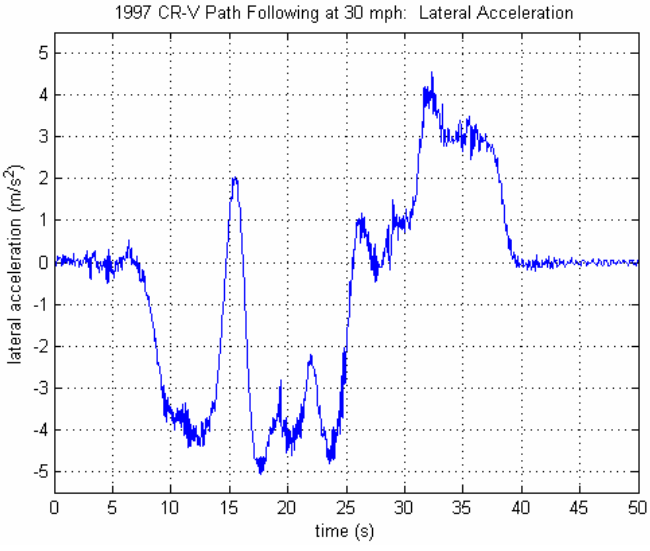

Fig. 28: CR-V path following at 30 mph (48 kph)

CONCLUSION

An automated steering controller, capable of both open-loop handwheel maneuvers and closed-loop path following, has potential to improve the accuracy and repeatability of dynamic test inputs, as well as sparing the human test driver from tedious or injurious duties. The steering controller described in this paper is lightweight, compact, and easy to install without permanent vehicle modification. The controller will adapt as necessary to the dynamic characteristics of the vehicle.

The path-following algorithm is based on the PD-control method proposed by Sidhu. Four different vehicles were simulated over various paths and speeds to evaluate each of the three control parameters employed in this algorithm. For the first parameter, K_d, it was determined that a constant value would work well for all vehicles at all speeds.

Optimal values for another parameter, lookahead (LA), can be calculated from a simple linear relationship to vehicle speed. Simulation shows that the same linear rule can be used for most light- and medium-weight vehicles. Experiment affirms the same conclusion for lookahead, though with somewhat lower values.

The optimal values for the final parameter, K_p, are more elusive. Simulation results for this parameter proved unreliable, due likely to poor fidelity of the system model. K_p values calculated from a experimentally-derived yaw gain may prove a better guide, but further testing at higher speeds will be necessary to determine the appropriate rule. Otherwise, some adaptive mechanism such as model-reference adaptive control (MRAC) may be used to establish a K_p gain schedule for a particular vehicle.

Employing the optimal gains, the controller demonstrated the ability to accurately follow random paths of various types. Sample plots show good path-following performance even as tires approached saturation. The ATD speed controller facilitated testing by providing accurate, stable testing speeds, typically within ±0.1 m/s of the desired speed at steady state.

REFERENCES

1. Stähle GmbH, D-75242 Neuhausen-Steinegg, Germany. http://www.stahle.com/
2. Anthony Best Dynamics, Ltd., Holt Road, Bradford on Avon, Wiltshire BA15 1AJ England. http://www.abd.uk.com/
3. Schmidt, R., Weisser, H., Schulenberg, P., and Goellinger, H., 2000, "Autonomous Driving on Vehicle Test Tracks: Overview, Implementation, and Results," *Proc. 2000 IEEE Intelligent Veh. Symp.*, Detroit, MI, pp. 152-155.
4. Weisser H., Schulenberg P., Gollinger H., Michler T., 1999, "Autonomous Driving on Vehicle Test Tracks:

Overview, Implementation, and Vehicle Diagnosis" *Proc. IEEE Conf. Intelligent Transport Systems*, pp. 62-67.

5. Hoess, A., Hosp, W., Doerfler, R., and Rauner, H., 1996, "Longitudinal Autonomous Vehicle Control Utilizing Access to Electronic Throttle Control, Automatic Transmission and Brakes," SAE Paper. No. 961009.
6. Maciuca, D.B., Gerdes, J.C., and Hedrick, J.K., 1994, "Automatic Braking Control for IVHS," Proc. Int'l Symp. on Adv. Veh. Contr. (AVEC '94), Tsukuba, Japan.
7. Brown, K.M., Heydinger, G.J., Guenther, D.A., and Bixel, R.A., "Integration of an Adaptive Control Strategy on an Automated Steering Controller," SAE Paper No. 2005-01-0393.
8. Heydinger, G.J., Bixel, R.A., Coovert, D.A., Brown, K.M., and Guenther, D.A., "Development of a Computer Controlled Automated Steering Controller," SAE Paper No. 2005-01-0394.
9. SEA Limited, Inc., 7349 Worthington-Galena Rd., Columbus, OH, 43085. http://www.sealimited.com.
10. Sidhu, A., Mikesell, D.R., Guenther, D.A., Bixel, R., Heydinger, G., "Development and Implementation of a Path-Following Algorithm for an Autonomous Vehicle," SAE Paper No. 2007-01-0815.
11. Oxford Technical Solutions Ltd., 77 Heyford Park, Oxfordshire, OX25 5HD, UK. http://www.oxts.com/.
12. National Instruments Corp., 11500 N Mopac Expwy, Austin, TX 78759, http://www.ni.com/compactrio/.
13. Rankin, A., Crane, C., Armstrong, A., Nease, A., and Brown, H.E., 1996, "Autonomous Path Planning Navigation System Used for Site Characterization," *Proc. SPIE 10th AeroSense Symp.*, pp. 176-186, Orlando, FL, 1996.
14. Coulter, R.C., "Implementation of the Pure Pursuit Path Tracking Algorithm," Carnegie Mellon Robotics Institute Technical Report, CMU-RI-TR-92-01, 1992.
15. Wit, J., Crane, C.D. III, and Armstrong, D., "Autonomous Ground Vehicle Path Tracking," *Journal of Robotic Systems*, **21** (8), pp. 439-449, 2004.
16. Gillespie, T.D., 1992, *Fundamentals of Vehicle Dynamics*, SAE, Inc., Warrendale, PA, Chap. 6.
17. Bedner, E., Fulk, D., and Hac, A., "Exploring the Trade-Off of Handling Stability and Responsiveness with Advanced Control Systems," SAE Paper No. 2007-01-0812.
18. Wilde, J.R., 2005, "Experimental Evaluation and ADAMS Simulation of the Kinetic Suspension System," M.S. Thesis, Ohio State University, Columbus, OH.

CONTACT

David R. Mikesell is a Ph.D. candidate at Ohio State University (mikesell.13@osu.edu). He has accepted a faculty appointment in Mechanical Engineering at Ohio Northern University to begin August 2007.

APPENDIX

3-DOF Model of Vehicle Lateral Dynamics

$$\begin{bmatrix} m & 0 & m_s h & 0 \\ 0 & I_{zz} & I_{xz} & 0 \\ m_s h & I_{xz} & I_{xx} & 0 \\ 0 & 0 & 0 & 1 \end{bmatrix} \begin{bmatrix} \dot{V} \\ \dot{r} \\ \ddot{\phi} \\ \dot{\phi} \end{bmatrix} = \begin{bmatrix} F_{Y_V} & F_{Y_r} & 0 & F_{Y_\phi} \\ M_{Z_V} & M_{Z_r} & 0 & M_{Z_\phi} \\ 0 & M_{X_r} & -B_f - B_r & M_{X_\phi} \\ 0 & 0 & 1 & 0 \end{bmatrix} \begin{bmatrix} V \\ r \\ \dot{\phi} \\ \phi \end{bmatrix} + \begin{bmatrix} F_{Y_\delta} \\ M_{Z_\delta} \\ 0 \\ 0 \end{bmatrix} \delta_K \quad (9)$$

Coefficients for the above equation are defined as follows:

$$F_{Y_V} = -2\left(\frac{C_f' + C_r'}{U}\right)$$

$$F_{Y_r} = -mU - 2\left(\frac{aC_f' + bC_r'}{U}\right)$$

$$F_{Y_\delta} = 2C_f'$$

$$M_{Z_V} = -2\left(\frac{aC_f' - bC_r' - C_{Mf} - C_{Mr}}{U}\right)$$

$$M_{Z_r} = -2\left(\frac{a^2 C_f' - aC_{Mf}' + b^2 C_r' + bC_{Mr}}{U}\right)$$

$$M_{Z_\phi} = 2\left(\begin{matrix}\varepsilon_f\left(aC_f' - C_{Mf}'\right) - \varepsilon_r\left(b^2 C_r' + bC_{Mr}\right) + \\ C_\gamma\left(aC_{\phi_f} - bC_{\phi_r}\right)\end{matrix}\right)$$

$$M_{Z_\delta} = 2\left(aC_f' - C_{Mf}'\right)$$

$$M_{X_r} = -m_s hU$$

$$M_{X_\phi} = -K_f - K_r + m_s gh$$

$$C_f' = \frac{C_f}{1 + K_{mf} C_{mf} - K_{ff} C_f}$$

$$C_r' = \frac{C_r}{1 + K_{mr} C_{mr} - K_{fr} C_r}$$

$$I_{XZ} = m_s ch$$

	UNITS	VEHICLE PARAMETERS
m	kg	total vehicle mass
m_s	kg	sprung mass
I_{ZZ}	kg-m^2	total vehicle yaw moment of inertia
I_{XX}	kg-m^2	sprung mass roll moment of inertia
H_{CG}	m	total vehicle center of gravity height
h	m	vertical distance between roll axis and m_s
a	m	longitudinal distance from vehicle CG to front axle
b	m	longitudinal distance from vehicle CG to rear axle
c	m	longitudinal distance from vehicle CG to sprung mass CG
K_{Ff}	rad/N	front lateral force suspension compliance steer
K_{Fr}	rad/N	rear lateral force suspension compliance steer
K_{Mf}	rad/(Nm)	front aligning torque suspension compliance steer
K_{Mr}	rad/(Nm)	rear aligning torque suspension compliance steer
ε_f	deg/deg	front roll steer
ε_r	deg/deg	rear roll steer
$C_{\phi f}$	deg/deg	front camber to roll coefficient
$C_{\phi r}$	deg/deg	rear camber to roll coefficient
K_f	Nm/rad	front overall roll stiffness
K_r	Nm/rad	rear overall roll stiffness
B_f	Nm/(rad/s)	front overall roll damping
B_r	Nm/(rad/s)	rear overall roll damping
K_{sr}	rad/rad	handwheel steering ratio

	UNITS	TIRE PARAMETERS
$C_{\alpha f}$	N/rad	front tire cornering stiffness
$C_{\alpha r}$	N/rad	rear tire cornering stiffness
C_{Mf}	Nm/rad	front tire aligning moment stiffness
C_{Mr}	Nm/rad	rear tire aligning moment stiffness
C_γ	N/rad	tire camber stiffness

	UNITS	MODEL VARIABLES, STATES
V	m/s	lateral velocity
r	rad/s	yaw rate
ϕ	rad	roll angle
δ_K	rad	front tire steer angle
δ_{hw}	rad	handwheel steer angle